Kinetic analysis of transcellular passage of the cobalamin–transcobalamin complex in Caco-2 monolayers

Christian B. Juul[a,†], Sergey N. Fedosov[a,†,*], Ebba Nexo[b], and Christian W. Heegaard[a,*]
[a]Department of Molecular Biology and Genetics, Aarhus University, 8000 Aarhus, Denmark; [b]Department of Clinical Biochemistry, Aarhus University Hospital, 8200 Aarhus N, Denmark

ABSTRACT **We suggest a novel kinetic approach to quantifying receptor–ligand interactions via the cellular transport and/or accumulation of the ligand. The system of cobalamin (Cbl, vitamin B12) transport was used as a model, because Cbl is an obligatory cofactor, taken up by animal cells with the help of a transport protein and a membrane receptor. Bovine transcobalamin (bTC) stimulated the cellular accumulation and transcytosis of radioactive [^{57}Co]Cbl in polarized monolayers of Caco-2 cells. The bovine protein was much more efficient than human TC. The transport was inhibited in a dose-dependent manner by the unlabeled bTC-Cbl complex, the ligand-free bTC, and the receptor-associated protein (RAP). This inhibition pattern implied the presence of a megalin-like receptor. Quantitative assessment of kinetic records by the suggested method revealed the apparent concentration of receptors in vitro (≈15 nM), as well as the dissociation constants of bTC–Cbl (K_d = 13 nM) and RAP (K_d = 1.3 nM). The data were used to estimate the effective luminal concentrations of TC-specific receptors in kidneys (3.8 μM) and intestine (50 nM), the tissues resembling polarized Caco-2 cells.**

Monitoring Editor
Keith E. Mostov
University of California, San Francisco

Received: Sep 10, 2018
Revised: Nov 26, 2018
Accepted: Dec 14, 2018

INTRODUCTION

Characterization of membrane receptor binding activity is usually performed after isolation of the relevant membrane fraction, followed by solubilization and immobilization of the receptor in question. Disturbance of the natural environment, as well as various treatments, might change the affinity and create a false impression regarding receptor functionality under physiological conditions.

Among the eye-catching examples of a contradictory quantification of receptor–ligand interactions is the system of cobalamin (Cbl, vitamin B12) uptake in mammalian tissues. The uptake is mediated via interaction of the specific Cbl-transporting protein transcobalamin (TC) and the two known receptors of the TC–Cbl complex, CD320 and megalin. CD320 is assumed to be responsible for the ubiquitous cellular uptake of circulating TC–Cbl from blood (Quadros *et al.*, 2009), whereas the multifunctional receptor megalin (also known as LRP2) is apparently responsible for the renal reabsorption of TC–Cbl (Birn *et al.*, 2002). Previous examinations of membrane preparations, as well as solubilized or immobilized receptors, revealed a broad span of estimated dissociation constants with K_d = 0.02–6.7 nM for CD320 (Seligman and Allen, 1978; Nexo and Hollenberg, 1980; Quadros *et al.*, 1994, 2005) and K_d = 12–1400 nM for megalin (Moestrup *et al.*, 1996). This high dispersion apparently originates from 1) various techniques used to isolate the receptors and 2) disparate binding protocols used. A broad span of affinities adds some ambiguity concerning the receptor–TC interactions in vivo, because the concentration of TC–Cbl complex in blood and primary urine is low (typically below 0.2 nM). In addition, there are no estimates of the effective receptor concentrations in the luminal spaces of relevant

This article was published online ahead of print in MBoC in Press (http://www.molbiolcell.org/cgi/doi/10.1091/mbc.E18-09-0571) on December 19, 2018.
The authors declare that they have no conflict of interest.
[†]These authors contributed equally to this work.
*Address correspondence to: Sergey N. Fedosov (snf@mbg.au.dk); Christian W. Heegaard (cwh@mbg.au.dk).
Abbreviations used: Ado/Me/CN/HOCbl, 5′-deoxyadenosyl/methyl/cyano/hydroxocobalamin; b/hTC, bovine/human transcobalamin; Cbl, cobalamin (vitamin B12); [^{57}Co]Cbl, core moiety of radioactive Cbl; HC, haptocorrin; HO[^{57}Co]Cbl, radioactive form of HOCbl; IF, intrinsic factor; RAP, receptor-associated protein; TC, transcobalamin; TC–Cbl, transcobalamin–cobalamin complex; X[^{57}Co]Cbl, radioactive Cbl with an unspecified group.

tissues. The quantitative characterization of Cbl uptake is nevertheless important from several angles of view, as outlined below.

Cobalamins are water-soluble organometallic molecules with the same core structure of [Co^{3+}]Cbl, but differing in the cobalt-coordinated exchangeable group X—for example, cyanide (in the synthetic form CNCbl), water (in HOCbl), 5′-deoxyadenosyl (in AdoCbl), and methyl (in MeCbl; Kräutler and Puffer, 2012). The uptake of Cbl by humans is via a complex route, involving a number of specific protein transporters and receptors, reviewed in Fedosov (2012), Nielsen *et al.* (2012), and Green *et al.* (2017). Intestinal absorption of Cbl is usually achieved through the concerted action of the Cbl-binding protein intrinsic factor (IF) and the IF–Cbl receptor cubam. The transport from blood to body cells requires TC and CD320. Internalized Cbl with any X-group is gradually converted to its two coenzyme forms (AdoCbl and MeCbl), which are light-sensitive and easily produce the third natural form (HOCbl; Kräutler and Puffer, 2012). Insufficiency of Cbl causes inhibition of the related enzymes and eventually leads to megaloblastic anemia and/or neural disorders, if not treated in time (Green *et al.*, 2017).

Humans acquire Cbl from animal-derived products and vitamin supplements, which provide an ample amount of the vitamin (Watanabe, 2007; Fedosov, 2012) in comparison with the recommended daily dose of ≈2 nmol (≈2.7 µg; Green *et al.*, 2017). Accordingly, there is a general positive correlation between the intake of animal foods and Cbl status (Miller et al, 1991; Watanabe, 2007). Bioavailability of vitamin B12 from dietary sources is essentially determined by the properties of various Cbl-binding proteins present in food (Carmel, 1995; Watanabe, 2007). They usually constrain Cbl, especially if the proteins have a high resistance to digestion. Yet possible interactions of the Cbl-binding proteins with intestinal receptors (different from cubam) might facilitate uptake.

Cow's milk suggests an interesting potential alternative to the conventional transportation route, because approximately half of the endogenous Cbl in cow's milk is bound to TC (Fedosov *et al.*, 1996, 2018). The complex TC–Cbl might bypass the "normal" intestinal route if compatible receptors are present. Indeed, the ingestion of milk seems to be particularly beneficial in terms of B12 status, according to several population studies (Vogiatzoglou *et al.*, 2009; Matte *et al.*, 2012). Moreover, purified bovine TC (bTC) promoted accumulation of CNCbl by polarized Caco-2 monolayers (Hine *et al.*, 2014), a widely used model of the human small intestine epithelium (Ramanujam *et al.*, 1991; Bose *et al.*, 1997, 2007; Pons *et al.*, 2000; Hubatsch *et al.*, 2007). Earlier qualitative and semiquantitative data showed a considerable enhancement of Cbl transport (apical to basolateral) across Caco-2 monolayers upon addition of human IF (Ramanujam *et al.*, 1991; Pons *et al.*, 2000), as well as some enhancement in the presence of human TC (Bose *et al.*, 1997; Pons *et al.*, 2000). In contrast, the binding of Cbl to HC (Ramanujam *et al.*, 1991; Pons *et al.*, 2000) or the addition of anti-TC antibodies in the TC-related experiments (Pons *et al.*, 2000) suppressed the transcytosis.

The high importance of Cbl and the uncertain quantitative description of its receptor binding appeal to an approach that allows measurement of affinity and receptor content directly under the translocation of Cbl through a cell layer. We suggest for this purpose a computational kinetic method that relies on the measurement of accumulated/transported ligand. We demonstrate that the passage of radioactive HO[^{57}Co]Cbl through the Caco-2 monolayer is much more efficient when the ligand is bound to bovine TC rather than human TC. This observation might imply the possibility of an unusual transportation route for Cbl in the small intestine. Quantitative characterization of the receptor(s) content and ligand affinity is done, and inferences concerning the physiologically relevant tissues are discussed.

RESULTS

General scheme of the transcellular transport of Cbl

Figure 1 depicts the mechanism of transcellular transport of Cbl used in our work. It was chosen based on the principle of minimal sufficiency and can be regarded as a plausible simplification of a more complex process. The scheme is briefly outlined in the current paragraph, and a more detailed description can be found in *Materials and Methods*, under *Kinetics*. The model considers three transitions, $A \rightarrow A^* \rightarrow B \rightarrow C$. The first transition, $A \rightarrow A^*$ (with the rate v_0), is confined to the upper (apical) compartment (with the volume V_A = 1 ml) and describes transformation of the receptor-bound "substrate" (e.g., bTC–HO[^{57}Co]Cbl) to its modified form *A**, ready for cellular uptake. Equilibration of the receptor with its "substrate" and optional "inhibitors" affects the rate of $A \rightarrow A^*$ transition. The second step, $A^* \rightarrow B$ (with the rate constant k_1), reflects the uptake of *A** into the cellular compartment (Caco-2 monolayer, with the volume V_B = 10 µl). The third transition, $B \rightarrow C$ (with the apparent rate constant k_2), describes how the accumulated intermediate *B* is exported to the lower (basolateral) compartment (with the volume V_C = 1 ml). A few possible minor routes of bTC–Cbl transportation were ignored, such as direct crossing of the monolayer by bTC–Cbl or reabsorption of bTC/hTC–Cbl from the basolateral compartment, followed by backward transport to the apical compartment (Pons *et al.*, 2000; Hannibal *et al.*, 2018). The time-dependent

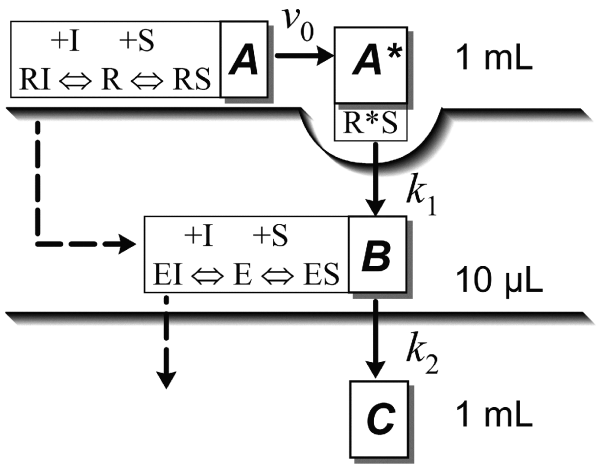

FIGURE 1: Scheme of TC–HO[^{57}Co]Cbl transport across a monolayer of cells. The first transition, $A \rightarrow A^*$ (solid arrow), goes with a velocity (v_0) and describes transformation of the receptor–substrate complex (RS), containing the bound TC–HO[^{57}Co]Cbl (S), to a complex R*S ready for cellular uptake. "*A*" denotes the total quantity of TC–HO[^{57}Co]Cbl in the upper (apical) compartment (volume V_A = 1 ml). "*A**" denotes TC–HO[^{57}Co]Cbl ready for cellular uptake. The presence of a competitive inhibitor (I), such as nonradioactive TC–Cbl, affects v_0. The second transition, $A^* \rightarrow B$, has a rate constant k_1 and describes the receptor–mediated cellular uptake of TC–HO[^{57}Co]Cbl, where "*B*" stands for the total radioactivity within the cellular compartment (volume V_B = 10 µl). The third transition, $B \rightarrow C$, has an apparent rate constant k_2 and describes the export of HO[^{57}Co]Cbl to the lower (basolateral) compartment (volume V_C = 1 ml). "*C*" denotes the total amount of radioactive tracer accumulated in V_C. The export is mediated by a specific transporter (E), affected by the presence of a competitive inhibitor (I), such as nonradioactive Cbl. The parallel transport of I (e.g., Cbl) is depicted by dashed arrows.

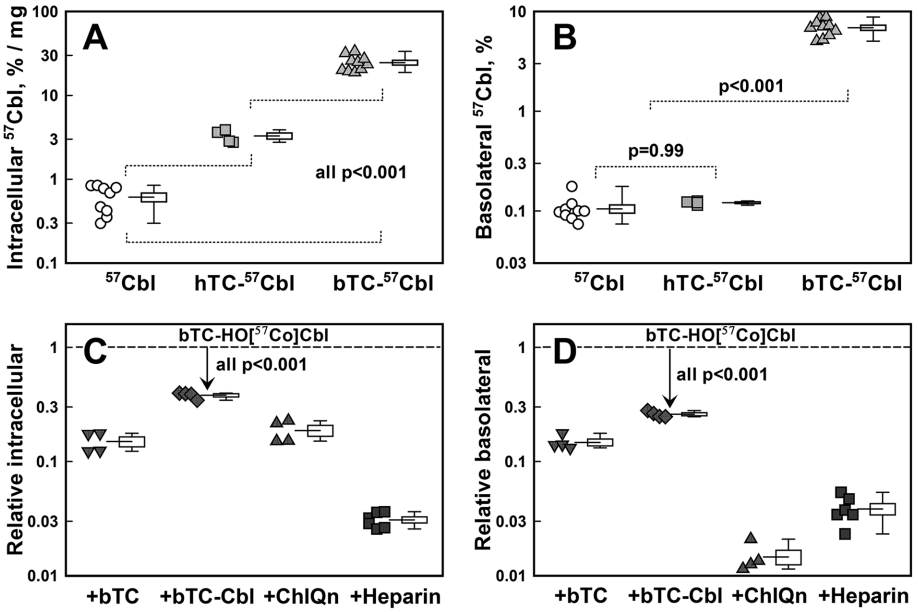

FIGURE 2: Effect of TC on the cellular transport of HO[^{57}Co]Cbl (10 h incubation) and examination of inhibitors. (A, B) Intracellular and transported radioactivity (in the respective panels) after addition of HO[^{57}Co]Cbl to the apical compartment without additives or with hTC or bTC. The *Y*-axis presents the percentage of the total radioactivity shown in a logarithmic scale. Symbols indicate the individual measurements, while the horizontal line/box/whiskers correspond to mean/SEM/range, respectively. Probabilities of pairwise identity between the data sets are indicated by braces (*p*, Tukey–Kramer test for multiple comparisons). (C, D) Inhibition of the intracellular and basolateral accumulation of radioactivity, respectively, in the presence of bTC, bTC–HOCbl, chloroquine, or heparin in the apical compartment. The *Y*-axis presents the decrease of measured values in relation to bTC–HO[^{57}Co]Cbl taken alone (baseline —). Other notation as in panels A and B. Probability of identity to the baseline is shown by an arrow (*p*, Dunnett test). For the details see the main text.

accumulation of *C* and the endpoint amount of *B* constituted the objects of our kinetic analysis.

Qualitative assessment of TC effects on HO[^{57}Co]Cbl transport

Several qualitative experiments were done to test the ability of two TC types (bovine and human) to promote the cellular uptake and the transcellular transport of HO[^{57}Co]Cbl by Caco-2 monolayers after 10 h of incubation. In the first setup, we compared the results for free HO[^{57}Co]Cbl and its preformed complexes with those for bTC or hTC (see *Materials and Methods*). The three ligands HO[^{57}Co]Cbl, hTC–HO[^{57}Co]Cbl, and bTC–HO[^{57}Co]Cbl were added to the apical compartment (pH 7.4), and accumulation and translocation were measured as percentages of total radioactivity, because the total concentration of added tracer varied from 10 to 16 nM due to technical details of different experiments (performed over several months). The intracellular and translocated counts after 10 h of incubation are shown in Figure 2, A and B. The intracellular counts (Figure 2B) were normalized to total protein content of cell lysates and expressed as percentages of the tracer per milligram of protein.

Intracellular accumulation of free apical HO[^{57}Co]Cbl (Figure 2A) was low but increased by factors of ≈5 and ≈40 when its complexes with hTC and bTC were preformed. Transcellular passage of free HO[^{57}Co]Cbl (Figure 2B) was low and did not change in the presence of hTC, at least within our time scale of 10 h (shorter than the 30 h employed by Pons *et al.*, 2000). Substitution of a semipurified human seminal TC for the recombinant hTC made no difference (n = 2; the data were pooled with recombinant hTC). In contrast, the transport increased by a factor of 65 when the bTC–HO[^{57}Co]Cbl complex was applied (Figure 2B, closed triangles). Some conjectures about the difference between hTC and bTC are presented in the *Discussion*.

A control experiment on permeability of the Caco-2 monolayer showed that its integrity was not affected by bTC. The apparent permeability coefficient P_{app} of D–[^{14}C]–mannitol in the presence and absence of bTC–HOCbl (16 nM) remained unchanged ($p = 0.49$), with respective values of $P_{app} = (1.81 \pm 0.05) \times 10^{-7}$ and $(1.83 \pm 0.03) \times 10^{-7}$ cm/s. Both coefficients are well below $P_{app} = 1 \times 10^{-6}$ cm/s, associated with a "leaking" monolayer (Hubatsch *et al.*, 2007).

Protein association patterns of transported basolateral Cbl

The translocated radioactivity was collected from the basolateral compartment between 6 and 10 h of incubation and corresponded to ≈280 pM of [^{57}Co]Cbl. The ligand was retrieved mainly as the protein-free [^{57}Co]Cbl (70%); see the gel filtration profile in Supplemental Figure S1A. The rest was bound to proteins with molecular weights of HC (14%) and TC (16%), whose origins were assessed further. The culture medium contained 1:10 thermoinactivated bovine serum, which provided the exceptionally heat-resistant bovine HC (Fedosov *et al.*, 1996) at a concentration of ≈40 pM plus a small amount of bTC ≈ 4 pM; see Supplemental Figure S1B. These "exogenous" proteins captured free [^{57}Co]Cbl and artificially increased the protein-bound radioactivity by ≈16%. Secretion of hTC by Caco-2 cells (≈3 pM/h to the apical chamber and ≈5 pM/h to the basolateral chamber; see Supplemental Figure S1C) further added ≈7% to the protein-bound pool. This material balance indicated that only a minor (≈7%) direct transfer of the original bTC–HO[^{57}Co]Cbl through the monolayer took place under the conditions used (corroborating our assumption about the insignificance of this route). The translocated [^{57}Co]Cbl remained unmodified, as judged from its ability to bind to the most specific carrier IF; see the elution profile in Supplemental Figure S1A.

Analysis of the [^{57}Co]Cbl binding patterns in the basolateral compartment also confirmed that the backward basolateral → apical transport of TC–Cbl was of low impact. Thus, only 16% of [^{57}Co]Cbl was bound to hTC/bTC in the basolateral compartment at a total concentration of [^{57}Co]Cbl ≈ 280 pM. At low ligand concentrations, presence of the "inert" binder HC (≈40 pM in the medium) guaranteed capture of the translocated free [^{57}Co]Cbl, preventing its binding to the gradually accumulating "active" transporter hTC.

Qualitative assessment of inhibitors

In a setup similar to that of the preceding section, we qualitatively examined the effects of several potential inhibitors on the cellular uptake and the transcellular transport of HO[^{57}Co]Cbl. The apical medium contained the "substrate" (bTC–HO[^{57}Co]Cbl ≈ 5–15 nM) and a fixed concentration of one or another inhibitor. The following compounds were used: 1) a fivefold molar excess of ligand-free bTC

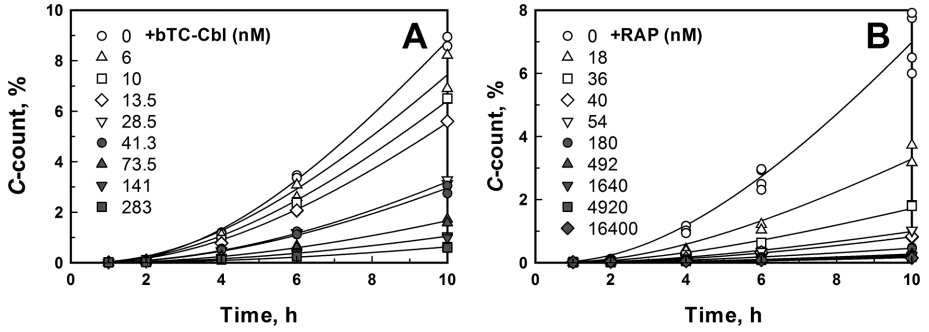

FIGURE 3: Time–dependent accumulation of radioactive Cbl in the basolateral compartment (*C* in % of total radioactivity added to the apical compartment) and the effect of inhibitors. (A) Suppression of transport by nonradioactive bTC–HOCbl. The apical compartment contained 1.5 nM of bTC–HO[^{57}Co]Cbl and 0–283 nM of the inhibiting complex bTC–HOCbl. (B) Suppression of transport by RAP. The apical compartment contained 18 nM of bTC–HO[^{57}Co]Cbl and 0–16,400 nM of RAP. All curves were approximated by Eq. 4.

(unsaturated TC binds to the receptor megalin [Moestrup *et al.*, 1996] but has a low affinity for CD320 [Quadros *et al.*, 2005]); 2) a fivefold molar excess of bTC–HOCbl (TC–Cbl binds to both receptors); 3) 75 μM of chloroquine (which inhibits clathrin-mediated endocytosis); and 4) 50 μg/ml heparin (a known binder of hTC; Fedosov *et al.*, 2005). The inhibiting effect (relative to the control with bTC–HO[^{57}Co]Cbl taken alone) was very noticeable for all compounds (n = 4 in each case) and covered both the intracellular accumulation (Figure 2C) and the transcellular transport of [^{57}Co]Cbl (Figure 2D). Earlier, the chloroquine-induced inhibition of TC–Cbl transcytosis was observed in Caco-2 monolayers by Pons *et al.* (2000) but not by Bose *et al.* (1997).

Kinetics of TC–HO[^{57}Co]Cbl transport and inhibition by TC–HOCbl and RAP

Increasing amounts of unlabeled bTC–HOCbl or receptor-associated protein (RAP; an antagonist of megalin binding [Moestrup *et al.*, 1996] with no effect on CD320 binding [Quadros *et al.*, 2009]) suppressed the transport of labeled bTC–HO[^{57}Co]Cbl in a dose-dependent way (Figure 3). The shapes of translocation curves (representing integrated radioactivity in the basolateral compartment traced over time) were consistent with the minimal kinetic scheme in Figure 1 (see also *Materials and Methods*, under *Kinetics*).

In the first set of experiments, we monitored the translocation of radioactivity (supplied as bTC–HO[^{57}Co]Cbl, called "substrate," with an apical concentration of s_0 = 1.5 nM) and the inhibition of this process by variable concentrations of its nonradioactive antagonist bTC–HOCbl (called "inhibitor," with apical i_0 = 0–282 nM). The respective records for accumulation of *C* in the basolateral compartment are shown in Figure 3A. The initial fits were done with the help of Eq. 4 under *Kinetics*, which included three floating parameters (v_0, k_1, and k_2). It was, however, found that the value of k_1 fluctuated around 1 h^{-1} without any particular correlation with the inhibitor concentration (preliminary fits are omitted). After a few trials, k_1 was fixed at 1.3 h^{-1}, which was reasonably consistent with both all *C*-curves in Figure 3A and the endpoint levels of intracellular radioactivity (*B*-curves in Figure 4; see the next section). The remaining floating parameters (v_0 and k_2) were calculated for each *C*-curve by fitting and used for the analysis of binding processes in the apical compartment (via v_0 values) and inside the cells (via k_2 values); see the corresponding sections. The final fitting curves are presented in Figure 3A as solid lines.

The second setup elucidated inhibition of the transcellular transport by RAP (Figure 3B). These experiments used higher concentrations of bTC–HO[^{57}Co]Cbl (fixed at s_0 = 18 nM), which in turn required an increase in RAP (i_0 = 0–16,400 nM). More radioactive tracer (s_0) was added, because the high-affinity binding of RAP gave the half-inhibition effect at a very low protein concentration (if using s_0 = 1.5 nM as in the bTC experiment; Figure 3A). The kinetic RAP–curves in Figure 3B were approximated by Eq. 4, where k_1 was set to 1.3 h^{-1} (see the preceding paragraph). The floating coefficients v_0 and k_2 were calculated by curve fitting and subjected to further analysis of the binding equilibria; see the relevant section.

Intracellular tracer accumulation and its inhibition by bTC–HOCbl and RAP

The intracellular radioactivity of [^{57}Co]Cbl was measured at the end of transport studies (10 h). The recovered percentage of total radioactivity was plotted versus the starting apical concentrations of bTC–HOCbl and RAP. Figure 4A presents the data plotted on a direct scale of ligand concentrations (within a shorter span), while Figure 4B depicts the full span of measurements shown in semilogarithmic coordinates. The experimental measurements (open symbols) are aligned with the theoretical values (closed symbols) predicted from the fitting of each *C*-curve in Figure 3. A good correspondence between the experimental data and the kinetic predictions (deduced from the kinetic events in other compartments) serves as additional validation of the model. The intracellular radioactivity (in the absence of inhibitors) corresponded to the intracellular concentrations of [^{57}Co]Cbl ≈ 15 nM in the bTC–HOCbl experiment (with a lower content of the substrate) and ≈160 nM in the RAP experiment

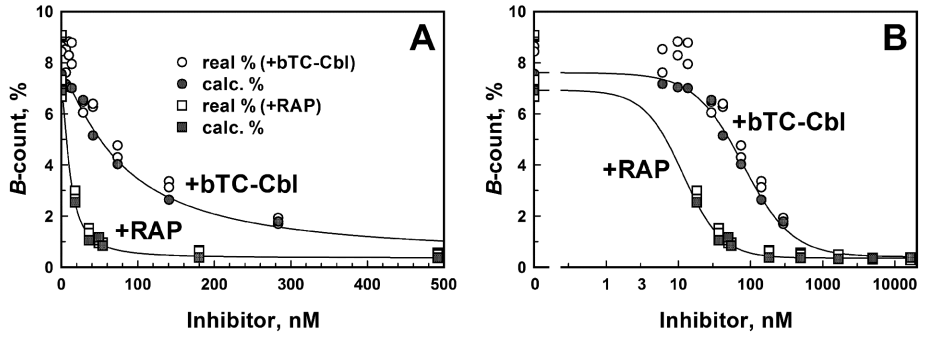

FIGURE 4: Accumulation of the radioactive ligand in the cells (*B* in % of the total radioactivity at 10 h) and the effect of inhibitors: nonradioactive bTC–HOCbl (circles) and RAP (squares). Open symbols show the experimental values; closed symbols depict predictions of the kinetic model based on the curve fitting in Figure 3. Concentrations of both inhibitors on the *X*-axis correspond to the apical compartment. (A) Short concentration scale, direct *X* coordinates. (B) Full concentration scale, logarithmic *X* coordinates.

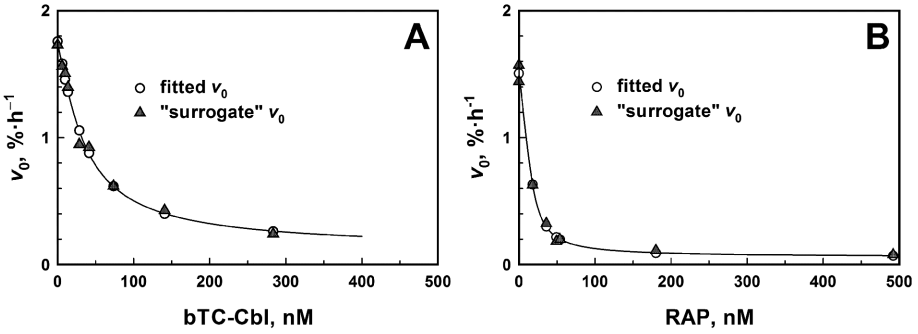

FIGURE 5: Inhibition of the receptor transformation velocity v_0 by (A) nonradioactive bTC–HOCbl and (B) RAP. Circles indicate v_0 values obtained from the transcellular transportation curves in Figure 3. Triangles show the "surrogate" v_0 based on single measurements of the transported radioactivity (10 h in Figure 3) combined with the intracellular radioactivity (Figure 4). All curves were fitted by Eq. 6.

(where a higher content of the substrate was used). The usual steady state concentrations of Cbl in animal tissues range from 10 nM (e.g., in the muscles) to 1000 nM (e.g., in the liver), as reviewed by Watanabe (2007) and Fedosov (2012).

Extracellular receptor binding of bTC–HOCbl and RAP in the apical compartment

The data on the inhibition of transport (Figure 3) and the intracellular accumulation of bTC–HO[^{57}Co]Cbl after 10 h of incubation (Figure 4) helped to quantify the binding equilibria in the upper (apical) compartment. We used for this purpose the rate v_0 calculated in two variants: 1) according to the curve fitting in Figure 3 (Eq. 4 was used) and 2) from a single 10-h measurement of the summed radioactivity, covering the intracellular counts (Figure 4) and counts transcytosed into the lower (basolateral) compartment (Figure 3). The result of second evaluation was called a "surrogate" v_0; see the substantiation in Eq. 5. Both assessments of v_0 represented the actual data assessed by two different calculation techniques, which were expected to give similar results (if the model did not contain an internal contradiction). The points in Figure 5 did not show any conspicuous difference from each other and were overlaid. Approximation of the pooled data sets was done using Eq. 6. This equilibrium saturation function allows calculation of both the dissociation constant(s) (K_s and/or K_i) and the apparent concentration of the binding sites (e_0), when their values are comparable under the experimental conditions (see *Materials and Methods*, under *Equilibrium reactions*).

Inhibition of transport by bTC–HOCbl (Figure 5A) was characterized by the following parameters: $F_0 = 1.75 \pm 0.02\%{\cdot}h^{-1}$ (i.e., v_0 without the inhibitor), $\Delta F = -1.64 \pm 0.05\%{\cdot}h^{-1}$ (the maximal amplitude of v_0 changes), $e_0 = 14.0 \pm 2.1$ nM (the receptor concentration in the apical compartment), and $K_s = K_i = 12.9 \pm 4.5$ nM (the dissociation constants of bTC–HO[^{57}Co]Cbl and bTC–HOCbl complexes, assumed to be identical to each other). All fitting results are shown as the optimal value ± SE.

The analogous analysis for RAP is presented in Figure 5B. Fitting was done using the stipulated value of $K_s = 12.9$ nM (the dissociation constant of bTC–HOCbl determined in the preceding paragraph). The other parameters were assessed by fitting as $F_0 = 1.51 \pm 0.01\%{\cdot}h^{-1}$, $\Delta F = -1.45 \pm 0.02\%{\cdot}h^{-1}$, $e_0 = 18.0 \pm 1.2$ nM, and $K_i = 1.31 \pm 0.18$ nM, indicating that RAP binds to the Caco-2 surface receptor ~10-fold more strongly than bTC–HOCbl. A small difference in receptor concentrations (e_0) in bTC and RAP experiments was ascribed to a slight variation in the cell number.

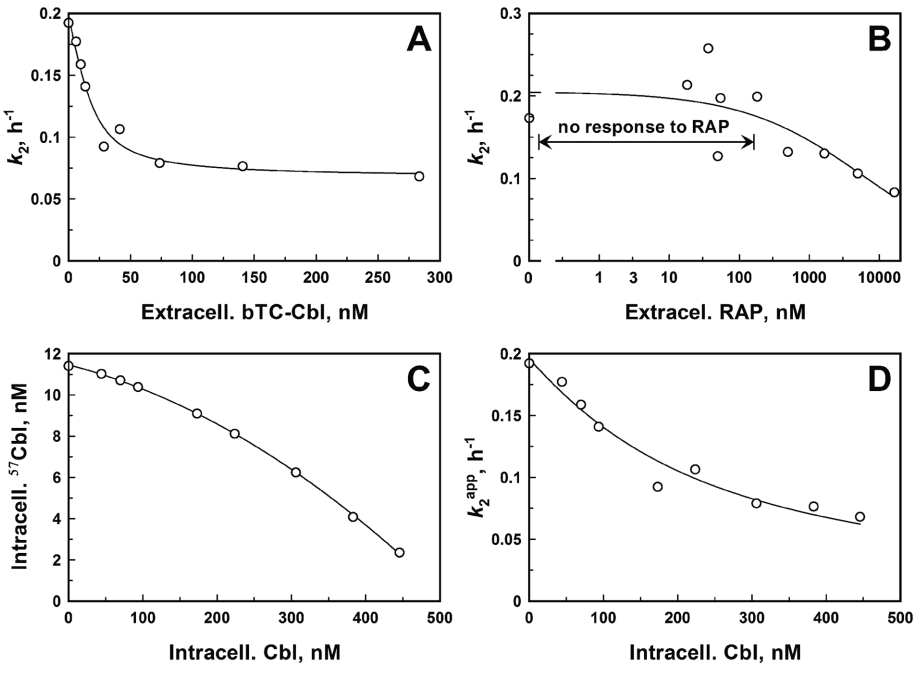

FIGURE 6: Inhibition effects of nonradioactive bTC–HOCbl and RAP inside the intracellular compartment. Response of the cellular secretion rate constant k_2 to (A) extracellular bTC–HOCbl and (B) extracellular RAP; both data sets are approximated by empirical curves. (C) Connection of the intracellular HO[^{57}Co]Cbl and the intracellular nonradioactive HOCbl by Eq. 8. (D) Dependence of the transportation parameter k_2 on the intracellular inhibitor (nonradioactive HOCbl). The curve was fitted by Eq. 6.

Intracellular events of [^{57}Co]Cbl secretion to the basolateral compartment

Secretion of HO[^{57}Co]Cbl (and possibly minor amounts of processed Ado[^{57}Co]Cbl and Me[^{57}Co]Cbl) from the monolayer to the basolateral compartment is governed by the parameter k_2 (Figure 1), determined from the kinetic curves in Figure 3. The nonradioactive complex bTC–HOCbl noticeably decreased k_2 within the lower range of its apical concentrations, <50 nM (Figure 6A). Such sensitivity of the kinetic "constant" to inhibition confirms its apparent status (conjectured in the model) and exposes competitive relationships between the radioactive tracer HO[^{57}Co]Cbl and the nonradioactive HOCbl inside the cell. The inhibiting effect of RAP on k_2 was marginal at low-to-moderate apical concentrations of 0–500 nM (Figure 6B), probably because of the lysosomal degradation of endocytosed RAP (Czekay *et al.*, 1997), with no consequence for the intracellular medium. Some

decrease in k_2 at a very high concentration of RAP (corresponding to protein ≈ 0.1–1 mg/ml) was regarded as nonspecific.

We used the percentage of intracellular radioactivity at 10 h of incubation (smoothing curve in Figure 4) to estimate the intracellular concentrations of HO[^{57}Co]Cbl and HOCbl based on the apical concentrations of bTC–HO[^{57}Co]Cbl and bTC–HOCbl (see Eqs. 7 and 8 in *Materials and Methods*). The two values were plotted versus each other in Figure 6C and used to quantify HOCbl–mediated inhibition of the intracellular transporter E (e.g., multidrug resistance protein 1 [MRP1]; Beedholm-Ebsen *et al.*, 2010), which participates in the secretion of Cbl into the lower compartment. For this purpose, k_2 was plotted versus i_{cell} in Figure 6D, whereupon the chart was fitted by Eq. 6, either supplemented by Eq. 8 (to express s_{cell} as a function of i_{cell}) or using any small s_0 (see *Kinetics*). The two fitting procedures gave a total overlap of the curves and only marginal differences in the calculated parameters, assessed as $F_0 = -\Delta F = 0.193 \pm 0.01$ h^{-1} (starting value of k_2, equated to the negative total amplitude to stipulate the absent final level), $e_0 \approx 70 \pm 67$ nM (the intracellular concentration of transporter E), and $K_s = K_i \approx 110 \pm 102$ nM (the dissociation constant of Cbl from the intracellular transporter). The obtained values of e_0 and K_s corroborated the initial assumption of our kinetic model that the intracellular concentrations of [^{57}Co]Cbl ≤ 15 nM (bTC–HOCbl experiment) are considerably smaller than both e_0 and K_s, thereby making the layouts of Eqs. 3 and 4 acceptable in connection with their presentation of k_2 (stipulating no B terms within the k_2 function).

DISCUSSION

In the current study, we employed polarized monolayers of Caco-2 cells to analyze the ligand–receptor interactions under transcellular passage of Cbl, free or bound to TC. A kinetic model (Figure 1) was developed to quantify and interpret the transportation curves (Figure 3). The suggested method is generally applicable to transcellular trafficking and intracellular accumulation of ligands.

The two tested carriers bTC and hTC (of bovine and human origin, respectively) behaved differently in promoting the uptake of Cbl (Figure 2A) and its transcellular transport (Figure 2B). It appeared that bTC was much more efficient, especially under the transcellular passage. The difference between bTC and hTC might be associated with different pI values of the two proteins (9.22 and 6.29, respectively). A positive charge of bTC at neutral pH should stabilize it at the negatively charged cell membrane surface, facilitating the subsequent encounter with the specific receptor. We also found that facilitated uptake of bTC–Cbl was approximately fourfold higher than previously reported by other authors, who used a rather low degree of TC–saturation by Cbl (16%; Hine *et al.*, 2014), in comparison to our assay (≥90%). The presence of excessive ligand-free bTC should cause a noticeable inhibition of bTC–Cbl uptake, as follows from our data in Figure 2, C and D.

The original bTC apparently degraded upon translocation of [^{57}Co]Cbl, because nearly all radioactivity in the basolateral compartment (≈93%) was associated with protein-free [^{57}Co]Cbl, counting here both the "truly free" ligand and its fractions recaptured by the specific proteins in the medium. Basolateral liberation of free Cbl implies the lysosomal processing of endocytosed TC–Cbl, observed in different epithelial cells (see Pons *et al.*, 2000; Hannibal *et al.*, 2018, and references therein). The lysosomal mechanism was confirmed in our study by a noticeable inhibition of the transport by chloroquine (Figure 2, C and D), also observed by Pons *et al.* (2000) but not by Bose *et al.* (1997).

The transportation of bTC–HO[^{57}Co]Cbl complex by the Caco-2 cells is probably receptor-mediated, and not caused by a facilitated unspecific passage through the monolayer, as was also stated by other authors (Bose *et al.*, 1997, 2007; Pons *et al.*, 2000). This conclusion follows from the aforementioned release of processed free [^{57}Co]Cbl on the basolateral side, as well as from inhibition of the transport by bTC–Cbl and bTC (exposing competition for a receptor). Even more pronounced inhibition was caused by RAP (Figure 3, A and B), a specific ligand antagonist that interacts with the LDL receptor family (Czekay *et al.*, 1997). The observed effects of the unsaturated bTC (Figure 2, C and D) and RAP exclude one of the possible receptor candidates (CD320), because it shows poor recognition of both proteins (Quadros *et al.*, 2009). This in turn suggests that megalin might be responsible for recognition of bTC in Caco-2 cells, because this receptor binds RAP and does not discriminate between the saturated and unsaturated forms of TC (Moestrup *et al.*, 1996, and references therein).

Expression of megalin in the animal intestinal tissues has been reported earlier (Birn *et al.*, 1997; Yammani *et al.*, 2001), though there is no clear consensus in this regard (Jensen *et al.*, 2014). Notably, immunoblotting analysis of apical versus basolateral plasma membrane fractions from polarized Caco-2 cells indicated that megalin was present in the apical fragments (Bose *et al.*, 2007), though the authors ascribed recognition of hTC to a megalin-associated protein, "TC–R." Our immunocytochemical staining of the filter-grown Caco2 cells also revealed megalin in the apical membrane (Juul, 2017). Obviously, the possibility that a novel megalin-like receptor (coexisting with megalin in the apical membrane of Caco-2 cells) is at play cannot be excluded.

Previously reported affinities of (semi)purified megalin for TC and RAP vary within a broad range of values, apparently reflecting different treatments and immobilization techniques (Moestrup *et al.*, 1996). In our setup, the megalin-like receptor and its ligands interacted with each other in the apical compartment of Caco-2 chamber as a close proxy for the natural environment, providing the best imitation of the functionally relevant binding to date. Analysis of the translocation curves (Figure 3), supplemented by the intracellular accumulation of [^{57}Co]Cbl (Figure 4), allowed reconstruction of the binding events in the apical compartment (Figure 5), if suitable kinetic equations were used (shown in *Kinetics*). The current measurements indicated a high affinity of bTC–Cbl for the megalin-like receptor in the functioning Caco-2 cells ($K_d \approx 13$ nM), which matches that of iodinated rabbit TC added to megalin in a microwell experiment (Moestrup *et al.*, 1996).

Our setup allowed titration of the apical receptor sites, because their "active/apparent" concentration was comparable to that of the ligands and their dissociation constants. The apparent receptor concentration of ≈15 nM (corresponding to the "chemical activity" of surface receptors in a given volume) was measured in 1 ml of the apical compartment exposed to the growth surface of 3.14 cm^2. The above geometric dimensions (also shown in Supplemental Figure S2) give a surface/volume ratio (S/V) of 0.314 mm^{-1}, and this result can be used to predict the efficient concentrations of the TC receptor in the small intestine with a diameter of $d = 25$ mm (Helander and Fandriks, 2014) and renal proximal tubules with $d = 0.05$ mm (Homan *et al.*, 2016), if the receptor-expressing surfaces of these tissues indeed resemble Caco-2 cells. We should mention in this regard that the polarized epithelial cells of different origin share many morphological and transport characteristics, as was demonstrated during comparison of Caco-2 and Madin–Darby canine kidney monolayers (e.g., Bittermann and Goss, 2017, and references thereof). The surface of the small intestine should be further increased by a factor of 6.5 (Helander and Fandriks, 2014) because of additional villi folding, absent in Caco-2 cells and epithelial cells of proximal tubules (where

only a microvilli brush border exists). The *S/V* of an open tube depends only on its radius (*r*) according to the standard geometric expression $S/V = 2/r$. Simple calculations give the ratios of 6.5 × 2/12.5 = 1.04 mm^{-1} for the intestine and 2/0.025 = 80 mm^{-1} for the renal proximal tubules. A comparison to $S/V = 0.314$ mm^{-1} in the apical compartment of a Caco-2 monolayer (containing ≈15 nM of the megalin-like receptor) gives an estimate of the apparent concentration of this receptor in the intestinal lumen (≈50 nM), as well as in the renal tubules (≈3800 nM).

The performed assessment of the apparent receptor concentrations and the ligand affinities predicts that ~80% of 1.0–1.5 nM bTC–Cbl in cow's milk will bind to megalin (megalin-like receptor) in the intestinal tract if bTC can survive proteolysis long enough to interact with the receptor. The latter requirement is rather difficult to fulfill, however. The dissociation of Cbl from bTC at pH 2 (Fedosov *et al.*, 1996; stomach conditions) and the presence of a large number of Lys and Arg residues (trypsin targets) in the bTC sequence (Fedosov *et al.*, 1999) make unprotected bTC an unlikely candidate to deliver Cbl. Theoretically, the protein can be partially protected by milk matrix, especially if secretion of gastric acid and proteolytic enzymes is decreased. For example, a possibility of bTC-mediated uptake can be conjectured for patients with compromised digestion, common in the elderly. Some authors claim detection of the native iodinated TC in portal blood of rats after oral administration of ^{125}I–TC–Cbl (Bose *et al.*, 1997), though the quantity of translocated TC has not been assessed.

The critical role of megalin in the kidney is better established (Birn *et al.*, 2002). Here we assess the apparent concentration of "active" megalin in the kidney tubules (3.8 µM). A small diameter of kidney tubules gives a high *S/V*, which guarantees a high apparent concentration of the receptor and an efficient binding of nearly any ligand, such as 80% binding of a low-affinity ligand with $K_d = 1$ µM.

Regarding the intracellular content of Cbl, we made an attempt to evaluate the interaction of Cbl with protein(s), responsible for transfer of Cbl to the basolateral medium. The performed analysis pointed to ≈70 nM intracellular concentration of this transporter (likely to be MRP1), which bound free Cbl with the estimated dissociation constant $K_d \approx 110$ nM. To the best of our knowledge, this kind of calculation has not been performed previously. It should be noted that all intracellular Cbl was treated as a ligand present within the same intracellular compartment, even though Cbl is likely to be divided between several compartments, exchanging with the ligand at unknown rates. Therefore, the binding characteristics of the intracellular transporter E should be treated with some caution. An experiment with inside-out vesicles containing MRP1 pointed to K_d = 6–23 µM for different Cbl forms (Beedholm-Ebsen *et al.*, 2010), though it is difficult to imagine any significant binding of intracellular Cbl (10–100 nM in most tissues) at such high K_d values.

In summary, we suggest a novel kinetic method for assessing receptor–ligand binding in the polarized cells under uptake and translocation of a ligand (here Cbl). We found that bovine transcobalamin considerably enhanced transcytosis of Cbl through the Caco-2 monolayer, and this process was assisted by a RAP-sensitive megalin-like receptor. Inferences about the binding interactions were suggested for the relevant tissues.

MATERIALS AND METHODS

Materials

CN[^{57}Co]Cbl (0.41 µCi/pmol) was purchased from MP Biomedicals (Santa Ana, CA). CN[^{57}Co]Cbl was converted into HO[^{57}Co]Cbl by photoaquation as previously described (Kornerup *et al.*, 2016). D-[1-^{14}C]-mannitol (56.8 mCi/mmol) was purchased from Perkin Elmer (Waltham, MA). The human colorectal adenocarcinoma cell line Caco-2 (passage 29) was obtained from DSMZ (Braunschweig, Germany). Cell culture medium (DMEM Glutamax) and bovine serum were from Life Technologies (Carlsbad, CA). The BCA protein assay kit was from Pierce Biotechnology (Waltham, MA). Recombinant bovine and human TCs were expressed in *Pichia pastoris* and further processed as detailed earlier (Fedosov *et al.*, 1999, 2000). Recombinant human IF was obtained as described elsewhere (Fedosov *et al.*, 2003). Semipurified human TC was obtained from seminal fluid as previously described (Hansen and Nexo, 1992). Human recombinant RAP was expressed in *Escherichia coli* and purified as described earlier (Nykjaer *et al.*, 1992). Complete protease inhibitor tablets were from Roche (Basel, Switzerland). Ni–NTA resin was purchased from G Biosciences (St. Louis, MO). EDTA-free SigmaFAST protease inhibitor tablets, heparin from porcine intestinal mucosa, chloroquine, and all standard compounds were purchased from Sigma-Aldrich (St. Louis, MO).

Preparation of TC–HO[^{57}Co]Cbl complex

The complex of recombinant TC (bovine or human) and radioactive HO[^{57}Co]Cbl was prepared in the course of at least 15 min coincubation in the culture medium (22°C) before the cell experiments. The radioactive ligand contained a minor fraction of HO[^{57}Co]Cbl (35–40 pM, 500–650 Bq/ml) plus a major fraction of HOCbl (1 nM or more), regarded as a single pool. The TC sample contained 1.1 molar excess binding capacity.

Cell culture

Caco-2 cells were grown to 50–60% confluence in DMEM Glutamax cell culture medium, which contained 4 µg/ml folate (specifications) and no vitamin B12 (specifications and measurements), as far as the cofactors of one carbon metabolism were concerned. The medium was supplemented with 10% heat-inactivated fetal bovine serum (FBS; 20 pM B12 in the original serum), 100 U/ml penicillin, and 100 µg/ml streptomycin. The other conditions included humidified 5% CO_2/95% air atmosphere at 37°C. The culture medium was replaced every second day. The cells were subcultured by trypsinization with 0.25% trypsin and 0.9 nM EDTA in Dulbecco's phosphate-buffered saline (PBS) without Mg^{2+} or Ca^{2+} (DPBS–).

The Caco-2 cells used for transport studies were seeded in Nunc cell culture inserts (growth area 3.14 cm^2, pore size 0.4 µm; Thermo Fisher Scientific, Waltham, MA) at a density of ~2.25×10^5 cells/insert. The seeded cells were cultured in growth medium (1 ml apically and 2 ml basolaterally) with changes of medium 16 h after seeding and then every second day.

Cbl transport studies

Caco-2 cells (passage 32–42) were grown for 3 wk on porous membranes in the upper compartment of a two-compartment system as described above. The integrity of monolayers was assessed by transepithelial electric resistance (TEER), measured with a Millicell ERS 2 V ohmmeter (Millipore) and transepithelial flux of D-[1-^{14}C]-mannitol (see below). Caco-2 monolayers with TEER values above 900 ohm cm^2 were used for transport studies. Cbl transport studies were performed under humidified 5% CO_2/95% air at 37°C with complete culture medium (1 ml) in the basolateral compartment.

The apical incubation solution (1 ml of the complete culture medium) contained a constant initial concentration of the preformed complex of TC–HO[^{57}Co]Cbl or free HO[^{57}Co]Cbl and various initial concentrations of unlabeled TC–HOCbl and TC; see *Results* for further details. Samples of free HO[^{57}Co]Cbl were prepared by adding unlabeled HOCbl (10–15 nM) to the complete culture medium

15 min before adding free radiolabeled HO[^{57}Co]Cbl (500–650 Bq/ml). This scheme was chosen because the complete culture medium possessed a minor binding capacity for free Cbl (40–50 pM). The whole mixture was regarded afterward as a "radioactive substrate," disregarding the binding of a small fraction of HOCbl. In samples supplemented with chloroquine (75 μM), heparin (50 μg/ml), or RAP (up to 16400 nM), these compounds were coincubated with bTC–HO[^{57}Co]Cbl in the complete culture medium.

Basolateral samples of transported HO[^{57}Co]Cbl were collected at the indicated time points by replacement of the complete growth medium. The transport reaction was terminated by aspiration of the apical medium. The monolayers were rinsed twice with DPBS containing $MgCl_2$ and $CaCl_2$ (DPBS+) and the TEER values were measured. The cells were detached by trypsinization, washed three times in DPBS+ with protease inhibitors (Complete), and lysed by sonication (Branson SLPe sonifier). Aliquots of the solubilized cells were taken for measurement of protein and radioactivity. Protein quantification was done using the Pierce BCA Protein Assay Kit (Thermo Scientific). The amount of [^{57}Co]Cbl in the collected fractions (apical and basolateral media and cell lysates) was measured in equal volumes by gamma counting (Perkin Elmer/Wallac Wizard-2 2470 automatic gamma counter), and the results were adjusted to the total sample volume. Intracellular uptake and transcytosis of [^{57}Co]Cbl are presented as percentages relative to the total radioactivity recovered (the apical and basolateral media plus cell lysates) and normalized to the protein content of the cell lysate.

Gel filtration study

Size exclusion chromatography was done by high-performance liquid chromatography on a Superdex 200 column injected with 0.5 ml of the test medium containing the necessary additives (e.g., none, 10 nM IF, 161 pM HO[^{57}Co]Cbl). The elution buffer (pH 8.0) contained 0.1 M Tris, 1 M NaCl, 0.02% NaN_3, and 0.05% bovine albumin and was pumped at a rate of 0.4 ml/min.

D-[^{14}C]-mannitol permeability

Permeability of D-[^{14}C]-mannitol (3.5 μM) after 10 h with or without bTC–HOCbl (18 nM bTC and 16 nM HOCbl) was measured. Basolateral samples were counted in a scintillation counter and the apparent permeability coefficient (P_{app}, cm/s) was determined as

$$P_{app} = \frac{dQ/dt}{(AC_0)}$$

where dQ/dt is the steady state flux (cpm/s), A is the surface area of the cell culture insert membrane (3.14 cm^2), and C_0 is the initial concentration in the apical compartment (cpm/ml).

Statistical analysis

Results from transport experiments are presented as mean ± SEM. Multiple pairwise tests of the equal outcome (e.g., $A = B$, $A = C$, $B = C$) or multiple comparisons to the baseline set (A = baseline, B = baseline, C = baseline) were done by Tukey–Kramer and Dunnett tests, respectively. Curve fitting used the quasi-Newton least-squares method. All mathematical procedures employed KyPlot 5.0 (free software from KyensLab, Japan).

Cell dimensions

To estimate the volume and the surface area of the polarized Caco-2 cells, each cell was assumed to be a cylinder (diameter 5 μm, height 35 μm) supplemented by an apical brush border of microvilli (each microvillus being a smaller cylinder with diameter 0.1 μm and height 1.0 μm) as described in the literature (Crowe and Marsh, 1993; Crawley *et al.*, 2014; Helander and Fandriks, 2014); see also Supplemental Figure S2. The cells were arranged within a hexagonal lattice packing, which provides ~90.7% occupation of the total base surface (S = 3.14 cm^2). The total number of cells in the layer was therefore calculated from the ratio (base surface × 0.907)/(end face surface of one cell) = 1.45 × 10^7. The number of microvilli per cell (n = 375) was assessed using their linear dimensions and the surface enlargement factor (SEF = 13) measured on the average for the microvilli brush border in cells of the small intestine (Crawley *et al.*, 2014). This number is somewhat less than n = 566 in the tightest hexagonal packing of microvilli. The chosen measures and spatial arrangements provided additional reference values: volume of one cell (with apical brush border) = 690 μm^3; apical surface of the cell (without brush border) = 19.6 μm^2; apical surface of the cell (with brush border) = 255 μm^2. The total inner volume of the cellular compartment was finally estimated as ≈10 μl.

Kinetics: time-dependent reactions

The scheme in Figure 1 describes three transitions, $A \rightarrow A^* \rightarrow B \rightarrow C$, where the kinetic description of each compound is presented below.

Compound A. The radioactive ligand (HO[^{57}Co]Cbl ± TC) in the upper compartment constitutes A (given in percent), and its transition to A^* is described by a rate function v_0. This process goes via initial formation of the "inactive" receptor–substrate complex RS, which is further transformed to its "active" state R*S (ready for cellular uptake). The preliminary complex RS exists in a fast equilibrium involving the receptor "R," the substrate "S" (e.g., bTC–HO[^{57}Co]Cbl), and optionally the inhibitor "I" (e.g., bTC–HOCbl). It is plausible to assume that the total amount of all receptor forms on the cell surface (R + RS + RI) is constant, because the processes of endocytosis, recycling, destruction, and synthesis of novel receptors to some extent counterbalance each other. The transformation RS → R*S makes R*S partially or completely occluded within a membrane cavity (A^* is not a part of A). However, A^* is not part of the intracellular pool B either, assuming that R* loses S during washing (loss of ≤1% in total). The transformation $A \rightarrow A^*$ occurs at a nearly constant rate v_0 (at each given set of R, S, and I concentrations) because the overall decrease of bTC–HO[^{57}Co]Cbl in the apical compartment is low (≤15%), meaning that $A \approx$ constant. As a consequence, all RS-related fast equilibria remain unperturbed. The expression for v_0 can be written in several variants with the same physical meaning:

$$v_0 = -\frac{dA}{dt} = v_{+i} + v_{\infty i} = v_{-i} - v_{-i}\left(1 - \frac{v_{+i}}{v_{-i}}\right) + v_{\infty i}$$

$$= \left(v_{-i} + v_{\infty i}\right) - v_{-i}\left(1 - \frac{rs_{+i}}{rs_{-i}}\right)$$

The notation runs as follows: $v_{+i} = k_0 \cdot rs_{+i}$ and $v_{-i} = k_0 \cdot rs_{-i}$ are the respective rates of specific transformations in the presence and absence of inhibitor, both values being proportional to the concentration of RS complex (rs_{+i} and rs_{-i}); $v_{\infty i}$ is the rate of unspecific transformation in the presence of an infinitely high inhibitor (the mechanism is not specified). The sum of ($v_{-i} + v_{\infty i}$) corresponds to the overall rate v_0 at a given substrate concentration without any inhibitor, whereas v_{-i} equals the total amplitude of response to the inhibition. If the rate of unspecific transformation is very low ($v_{\infty i} \approx 0$), the inhibition starts from $v_0 = v_{-i}$ and ends at $v_0 \approx 0$. The final expression for v_0 is identical to the fitting Eq. 6 (see further, where the

advantages of such a presentation are discussed). The value of v_0 depends on the ligand concentrations, their dissociation constants, and the receptor concentration (all being components of the ratio rs_{+i}/rs_{-i}). Further information is given in *Equilibrium binding*.

Decrease in *A* can be described with help of Eq. 1:

$$A = A_0 - v_0 \cdot t \quad (1)$$

Here A_0 is the quantity of *A* at the starting point (100%); *t* is the time of reaction; and v_0 is the rate of change ($A \rightarrow A^*$) expressed as a percentage per time unit.

Compound A*. The turnover of "activated" receptor–substrate complex R*S (i.e., *A**) is determined by the balance between its production rate ($A \rightarrow A^*$, discussed in the preceding paragraph) and the rate of its cellular uptake ($A \rightarrow B$) in accordance with the following expressions:

$$\frac{dA^*}{dt} = v_0 - k_1 \cdot A^*$$

$$A^* = \frac{v_0}{k_1}\left(1 - e^{-k_1 t}\right); \quad k_1 = \frac{V_B}{V_A} k_1^{conc} \quad (2)$$

Here a new coefficient k_1 is introduced. This is the rate constant of mass transfer ($A^* \rightarrow B$) expressed as the reciprocal time, for example, h^{-1}. It should be noticed that the constant of mass transfer (k_1) depends on the compartment volumes and can be connected (if necessary) to the constant of concentration transfer (k_1^{conc}, independent of the volumes) as shown in the extension to Eq. 2, where V_A serves as a reference volume. The value of *A** increases exponentially from zero (at $t = 0$) to a plateau v_0/k_1 (at $t \rightarrow \infty$) with the time of half reaction $t_{½} = 0.693/k_1$. The plateau level remains unperturbed, as long as the changes in A_0 are insignificant.

Compound B. The intracellular quantity of bTC–HO[^{57}Co]Cbl (or just free HO[^{57}Co]Cbl, or both) is notated as *B* (expressed as a percentage). The rates of influx $A^* \rightarrow B$ (the uptake of bTC–HO[^{57}Co]Cbl from the apical compartment) and efflux $B \rightarrow C$ (the secretion of HO[^{57}Co]Cbl to the basolateral compartment) determine changes of *B* over time:

$$\frac{dB}{dt} = k_1 \cdot A^* - k_2 \cdot B; \quad (k_2) \cdot B = \left(k_2^{true} \frac{\omega_{(i)}}{3K_s + \omega_{(i)}} \right) \cdot S_{cell(B)}$$

Here a new mass transfer coefficient k_2 describes $B \rightarrow C$ secretion. The nature of k_2 is somewhat ambiguous without assessment of a ready data set. This coefficient might reflect either some unspecific membrane crossing (when k_2 is a true constant) or crossing via a specific transporter. In the latter case, k_2 is an apparent constant and depends on the ligand and the transporter concentrations. In our setup, we assumed that the intracellular concentration of S (HO[^{57}Co]Cbl) is much lower than the intracellular concentration of the transmembrane carrier E plus a relevant dissociation constant. This allows cancellation of S-concentrations from k_2, which becomes dependent only on the transporter and the inhibitor (nonradioactive Cbl). The latter is present at much higher concentrations and quickly reaches a pseudo–steady state (making $k_2 \approx$ constant over time). The physical interpretation of $k_2 \cdot B$ involves transformation of *B* to the intracellular concentration of the substrate s_{cell} (Eq. 7), an optional correction of the intracellular substrate for each inhibitor concentration (Eq. 8), or just stipulation of any small "insignificant" value of s_{cell} and incorporation of the ligand concentrations into Eqs. 6A–6D, containing the inhibitor-dependent element $\omega_{(i)}$, all discussed in the next sections. The function of k_2 can be transformed to a form identical with the expression for v_0 (discussed above) and fitting Eq. 6.

The kinetic function of *B* is described by Eq. 3:

$$B = \frac{v_0}{k_2}\left(1 - e^{-k_2 t}\right) - \frac{v_0}{k_2 - k_1}\left(e^{-k_1 t} - e^{-k_2 t}\right) \quad (3)$$

The curve of intracellular radioactivity (*B*) is a sigmoid. It starts from zero (at $t = 0$) and tends to a steady state plateau v_0/k_2 (at $t \rightarrow \infty$), assuming *A* and $v_0 \approx$ constant.

Compound C. The accumulated basolateral radioactivity (*C* as a percentage) is governed by the transition $B \rightarrow C$. The value of *C* follows from the overall material balance:

$$\Delta A = v_0 \cdot t = A^* + B + C$$

Considering the aforementioned expressions for *A** and *B* (Eqs. 2 and 3), the kinetic function of *C* (Eq. 4) is easily deducible:

$$C = v_0 \cdot t - \frac{v_0}{k_1}\left(1 - e^{-k_1 t}\right) - \frac{v_0}{k_2}\left(1 - e^{-k_2 t}\right) + \frac{v_0}{k_2 - k_1}\left(e^{-k_1 t} - e^{-k_2 t}\right) \quad (4)$$

Here the meaning of all parameters and variables is the same as in the preceding paragraphs. The appearance of *C* in the lower compartment should go with a noticeable lag, followed by an acceleration tending to a slope v_0 (reflecting a pseudo steady state, if $A \approx$ constant). The *C*-curves were used to assess all relevant parameters (v_0, k_1, and k_2) by nonlinear fitting.

Parameter v_0. The independent assessment of v_0 is also possible from a single point using the sum of *B* (intracellular radioactivity) and *C* (radioactivity in the lower basolateral compartment) measured after a sufficiently prolonged reaction:

$$B + C = v_0 \cdot t - \frac{v_0}{k_1}\left(1 - e^{-k_1 t}\right) \approx v_0 \cdot t, \quad (t \rightarrow 0) \quad (5)$$

The ratio $(B + C)/t$ gives the value of a "surrogate" velocity v_0 calculated from a single point (determined for a given combination of S and I).

Equation 5 can also be used for analysis of receptor–ligand interactions (reflected via the parameter v_0) if basolateral secretion is absent. In this case, measurement of the accumulated substrate (either over time or at $t \rightarrow \infty$) at different concentrations of some inhibitor would help to reconstruct a saturation curve like those in Figure 5.

Equilibrium reactions

Two parameters of the model in Figure 1 (v_0 and k_2) are not the real constants but depend on the respective rapid equilibria, EI ↔ I + E + S ↔ ES (where E stands for any binding protein). The scheme of competition between two ligands for a protein-binding site (when all compounds have similar concentrations comparable with their dissociation constants) was solved in the literature (Wang, 1995) and is used here in the adapted form. In each set of our kinetic experiments, the substrate was maintained at the same level but the concentration of inhibitor increased and caused a gradual decrease in the assessed factor according to Eq. 6:

$$f = F_0 - \Delta F\left(1 - \frac{es_{+i}}{es_{-i}}\right) \quad (6)$$

Here f is the measured factor (either v_0 or k_2 at a given concentration of the variable i_0); F_0 is the initial value of this variable (at $i_0 = 0$); ΔF corresponds to the maximal amplitude of response, where $f = F_0 - \Delta F$ (at $i_0 \to \infty$), and optionally $f = F_0 - F_0$ (at $i_0 \to \infty$); es_{+i} stands for the concentration of ES or RS in the respective S + I ligand mixtures ($es_{+i} = es_{-i}$ at $i_0 = 0$ and tends to zero at $i_0 \to \infty$); es_{-i} corresponds to the concentration of ES complex at a given concentration of S in the absence of I. Equation 6 looks somewhat cumbersome but gives two easy identifiable parameters, namely the start value (F_0) and the amplitude of response to inhibition (ΔF), simplifying the fitting procedure for other parameters.

The value of es_{+i} was expressed via a series of extending equations,

$$es_{+i} = \frac{s_0 \cdot \omega}{3K_s + \omega}; \quad \omega = 2 \cdot \cos\frac{\theta}{3} \cdot \sqrt{x^2 - 3y} - x \tag{6A}$$

$$\theta = \arccos\left(\frac{-2x^3 + 9 \cdot x \cdot y + 27 \cdot K_s \cdot K_i \cdot e_0}{2 \cdot \left(x^2 - 3y\right)^{3/2}}\right) \tag{6B}$$

$$x = K_s + K_i + s_0 + i_0 - e_0 \tag{6C}$$

$$y = K_s\left(i_0 - e_0\right) + K_i\left(s_0 - e_0\right) + K_s \cdot K_i \tag{6D}$$

where s_0, i_0, and e_0 are the total concentrations of S, I, and E in the corresponding compartments; K_s and K_i are the dissociation constants of ES and EI, respectively; and all other symbols in Eqs. 6A–6D represent "service" functions, expressed via s_0, i_0, e_0, and the dissociation constants.

The value of es_{-i} can be calculated via Eqs. 6A–6D at $i_0 = 0$, but an easier procedure involves a separate extending equation,

$$es_{-i} = 0.5 \cdot \left(e_0 + s_0 + K_s - \sqrt{\left(e_0 + s_0 + K_s\right)^2 - 4 \cdot e_0 \cdot s_0}\right) \tag{6E}$$

Equation 6 (together with all its extensions) can be used to determine the dissociation constants K_s and K_i and the concentration of binding sites e_0. The saturation functions for the intracellular compartment consider either any small s_0 (eliminated in a ratio of es_{+i}/es_{-i}) or an empirical function expressing s_0 for each particular i_0; see the next section.

Intracellular events of equilibrium reactions

The percentage of intracellular radioactivity at the end of the experiment (Figure 4) was used to calculate the intracellular concentration of HO[^{57}Co]Cbl and its nonradioactive competitor HOCbl (added as bTC–HOCbl to the apical compartment). It should be remembered that the two molecules are identical (except for radioactivity), and the percentage of uptake is expected to be the same for both compounds. We used the following expression for the intracellular concentrations of the substrate s_{cell} and the inhibitor i_{cell}, connected to the respective apical concentrations via Eq. 7:

$$x_{cell} = \frac{B(\%)}{100\%} \cdot x_0 \cdot \frac{V_{up}}{V_{cell}} \tag{7}$$

Here x_{cell} refers to either s_{cell} or i_{cell} (the intracellular concentrations); $B(\%)$ is the percentage of the radioactive tracer inside the cells; x_0 refers to either s_0 or i_0 (the respective concentrations in the apical compartment); and V_{up}/V_{cell} is the ratio between the volumes of the upper (apical) compartment (1 ml) and the intracellular space (0.01 ml). The two concentrations (s_{cell} and i_{cell}) were calculated, plotted versus each other in Figure 6C, and connected via an empirical function:

$$s_{cell}(\text{nM}) = 11.458 - 0.00926 \cdot i_{cell} - 2.538 \cdot 10^{-5} \cdot i_{cell}^2 \tag{8}$$

This Eq. 8 was inserted into Eq. 6 instead of the fixed value of s_0 to correct the effect of inhibitor (if any) on the intracellular s_{cell}. The alternative fitting procedures (s_{cell} fixed at any value below 15 nM) should not affect the outcome if the real transport is consistent with an assumption of $s_{cell} << e_0 + K_s$ (important for stipulation of k_2 as an s_{cell}-independent term).

ACKNOWLEDGMENTS

We warmly appreciate the competent technical assistance provided by Jette Fisker Pedersen and Inger Marie Jensen. This work is part of the TRIM Project supported by the Innovation Fund Denmark, Grant 0603–00518B (12-132437).

REFERENCES

Beedholm-Ebsen R, van de Wetering K, Hardlei T, Nexø E, Borst P, Moestrup SK (2010). Identification of multidrug resistance protein 1 (MRP1/ABCC1) as a molecular gate for cellular export of cobalamin. Blood 115, 1632–1639.

Birn H, Verroust PJ, Nexo E, Hager H, Jacobsen C, Christensen EI, Moestrup SK (1997). Characterization of an epithelial approximately 460-kDa protein that facilitates endocytosis of intrinsic factor–vitamin B12 and binds receptor-associated protein. J Biol Chem 272, 26497–26504.

Birn H, Willnow TE, Nielsen R, Norden AG, Bonsch C, Moestrup SK, Nexo E, Christensen EI (2002). Megalin is essential for renal proximal tubule reabsorption and accumulation of transcobalamin—B12. Am J Physiol Renal Physiol 282, F408–F416.

Bittermann K, Goss KU. (2017). Predicting apparent passive permeability of Caco-2 and MDCK cell-monolayers: A mechanistic model. PLoS One 12, e0190319.

Bose S, Kalra S, Yammani RR, Ahuja R, Seetharam B (2007). Plasma membrane delivery, endocytosis and turnover of transcobalamin receptor in polarized human intestinal epithelial cells. J Physiol 581, 457–466.

Bose S, Seetharam S, Dahms NM, Seetharam B (1997). Bipolar functional expression of transcobalamin II receptor in human intestinal epithelial Caco-2 cells. J Biol Chem 272, 3538–3543.

Carmel R (1995). Malabsorption of food cobalamin. Baillieres Clin Haematol 8, 639–655.

Crawley SW, Mooseker MS, Tyska MJ (2014). Shaping the intestinal brush border. J Cell Biol 207, 441–451.

Crowe PT, Marsh MN (1993). Morphometric analysis of small intestinal mucosa. IV. Determining cell volumes. Virchows Arch A Pathol Anat Histopathol 422, 459–466.

Czekay RP, Orlando RA, Woodward L, Lundstrom M, Farquhar MG (1997). Endocytic trafficking of megalin/RAP complexes: dissociation of the complexes in late endosomes. Mol Biol Cell 8, 517–532.

Fedosov SN (2012). Physiological and molecular aspects of cobalamin transport. Subcell Biochem 56, 347–367.

Fedosov SN, Berglund L, Nexo E, Petersen TE (1999). Sequence, S–S bridges, and spectra of bovine transcobalamin expressed in *Pichia pastoris*. J Biol Chem 274, 26015–26020.

Fedosov SN, Fedosova NU, Nexo E, Petersen TE (2000). Conformational changes of transcobalamin induced by aquocobalamin binding. Mechanism of substitution of the cobalt-coordinated group in the bound ligand. J Biol Chem 275, 11791–11798.

Fedosov SN, Laursen NB, Nexø E, Moestrup SK, Petersen TE, Jensen EØ, Berglund L (2003). Human intrinsic factor expressed in the plant *Arabidopsis thaliana*. Eur J Biochem 270, 3362–3367.

Fedosov SN, Nexo E, Heegaard CW (2018). Binding of aquocobalamin to bovine casein and its peptides via coordination to histidine residues. Int Dairy J 76, 30–39.

Fedosov SN, Orning L, Lovli T, Quadros EV, Thompson K, Berglund L, Petersen TE (2005). Mapping the functional domains of human transcobalamin using monoclonal antibodies. FEBS J 272, 3887–3898.

Fedosov SN, Petersen TE, Nexo E (1996). Transcobalamin from cow milk: isolation and physico-chemical properties. Biochim Biophys Acta 1292, 113–119.

Green R, Allen LH, Bjørke-Monsen AL, Brito A, Guéant JL, Miller JW, Molloy AM, Nexo E, Stabler S, Toh BH, *et al*. (2017). Vitamin B12 deficiency. Nat Rev Dis Primers 3, 17040.
Hannibal L, Bolisetty K, Axhemi A, DiBello PM, Quadros EV, Fedosov S, Jacobsen DW (2018). Transcellular transport of cobalamin in aortic endothelial cells. FASEB J 32, 5506–5519.
Hansen M, Nexo E (1992). Cobalamin binding proteins in human seminal plasma. Scand J Clin Lab Invest 52, 647–652.
Helander HF, Fandriks L (2014). Surface area of the digestive tract—revisited. Scand J Gastroenterol 49, 681–689.
Hine B, Boggs I, Green R, Miller JW, Hovey RC, Humphrey R, Wheeler TT (2014). Transcobalamin derived from bovine milk stimulates apical uptake of vitamin B12 into human intestinal epithelial cells. J Cell Biochem 115, 1948–1954.
Homan KA, Kolesky DB, Skylar–Scott MA, Herrmann J, Obuobi H, Moisan A, Lewis JA (2016). Bioprinting of 3D convoluted renal proximal tubules on perfusable chips. Sci Rep 6, 34845.
Hubatsch I, Ragnarsson EG, Artursson P (2007). Determination of drug permeability and prediction of drug absorption in Caco-2 monolayers. Nat Protoc 2, 2111–2119.
Jensen LL, Andersen RK, Hager H, Madsen M (2014). Lack of megalin expression in adult human terminal ileum suggests megalin-independent cubilin/amnionless activity during vitamin B12 absorption. Physiol Rep 2, e12086.
Juul CB (2017). Investigating the Effect of Bovine Transcobalamin on the Absorption of Cobalamin (Vitamin B12)—Studies in Cell Culture and the Rat. Ph.D. thesis, Department of Molecular Biology and Genetics, Aarhus University, Aarhus, Denmark, 150 pp.
Kornerup LS, Juul CB, Fedosov SN, Heegaard CW, Greibe E, Nexo E (2016). Absorption and retention of free and milk protein–bound cyano– and hydroxocobalamins. An experimental study in rats. Biochimie 126, 57–62.
Kräutler B, Puffer B (2012). Vitamin B_{12}-derivatives: organometallic catalysts, cofactors and ligands of bio-macromolecules. In: Handbook of Porphyrin Science, vols. 21–25, ed. KM Kadish, KM Smith, and R Guilard, Singapore/London: World Scientific, 133–263.
Matte JJ, Guay F, Girard CL (2012). Bioavailability of vitamin B12 in cows' milk. Br J Nutr 107, 61–66.
Miller DR, Specker BL, Ho ML, Norman EJ (1991). Vitamin B-12 status in a macrobiotic community. Am J Clin Nutr 53, 524–529.
Moestrup SK, Birn H, Fischer PB, Petersen CM, Verroust PJ, Sim RB, Christensen EI, Nexo E (1996). Megalin-mediated endocytosis of transcobalamin–vitamin-B12 complexes suggests a role of the receptor in vitamin-B12 homeostasis. Proc Natl Acad Sci USA 93, 8612–8617.
Nexo E, Hollenberg MD (1980). Characterization of the particulate and soluble acceptor for transcobalamin II from human placenta and rabbit liver. Biochim Biophys Acta 628, 190–200.
Nielsen MJ, Rasmussen MR, Andersen CB, Nexo E, Moestrup SK (2012). Vitamin B12 transport from food to the body's cells—a sophisticated, multistep pathway. Nat Rev Gastroenterol Hepatol 9, 345–354.
Nykjaer A, Petersen CM, Moller B, Jensen PH, Moestrup SK, Holtet TL, Etzerodt M, Thogersen HC, Munch M, Andreasen PA, Gliemann J (1992). Purified alpha 2–macroglobulin receptor/LDL receptor-related protein binds urokinase.plasminogen activator inhibitor type-1 complex. Evidence that the alpha 2–macroglobulin receptor mediates cellular degradation of urokinase receptor-bound complexes. J Biol Chem 267, 14543–14546.
Pons L, Guy M, Lambert D, Hatier R, Gueant J (2000). Transcytosis and coenzymatic conversion of [(57)Co]cobalamin bound to either endogenous transcobalamin II or exogenous intrinsic factor in caco-2 cells. Cell Physiol Biochem 10, 135–148.
Quadros EV, Nakayama Y, Sequeira JM (2005). The binding properties of the human receptor for the cellular uptake of vitamin B12. Biochem Biophys Res Commun 327, 1006–1010.
Quadros EV, Nakayama Y, Sequeira JM (2009). The protein and the gene encoding the receptor for the cellular uptake of transcobalamin-bound cobalamin. Blood 113, 186–192.
Quadros EV, Sai P, Rothenberg SP (1994). Characterization of the human placental membrane receptor for transcobalamin II–cobalamin. Arch Biochem Biophys 308, 192–199.
Ramanujam KS, Seetharam S, Ramasamy M, Seetharam B (1991). Expression of cobalamin transport proteins and cobalamin transcytosis by colon adenocarcinoma cells. Am J Physiol 260, G416–G422.
Seligman PA, Allen RH (1978). Characterization of the receptor for transcobalamin II isolated from human placenta. J Biol Chem 253, 1766–1772.
Vogiatzoglou A, Smith AD, Nurk E, Berstad P, Drevon CA, Ueland PM, Vollset SE, Tell GS, Refsum H (2009). Dietary sources of vitamin B-12 and their association with plasma vitamin B-12 concentrations in the general population: the Hordaland Homocysteine Study. Am J Clin Nutr 89, 1078–1087.
Wang ZX (1995). An exact mathematical expression for describing competitive binding of two different ligands to a protein molecule. FEBS Lett 360, 111–114.
Watanabe F (2007). Vitamin B12 sources and bioavailability. Exp Biol Med (Maywood) 232, 1266–1274.
Yammani RR, Seetharam S, Seetharam B (2001). Cubilin and megalin expression and their interaction in the rat intestine: effect of thyroidectomy. Am J Physiol Endocrinol Metab 281, E900–E907.